Calorimetric Signature of Quantum Measurement: A Record-Formation Heat Bound and Differential Microcalorimetry Test

Moses Rahnama *

Posted Date: 27 February 2026

doi: 10.20944/preprints202602.1739.v1

Keywords: quantum measurement; Landauer principle; thermodynamics of information; objective classical record; record formation; mutual information; decoherence; quantum Darwinism; circuit QED; superconducting qubits; differential microcalorimetry; nanocalorimetry

 doi:10.20944/preprints202602.1739.v1

Article

Calorimetric Signature of Quantum Measurement: A Record-Formation Heat Bound and Differential Microcalorimetry Test

Moses Rahnama

Mina Analytics, New York, United States; moses@minaanalytics.com

Abstract

We propose that the transition from reversible quantum correlation to an *objective classical record* is a thermodynamically irreversible process with a quantifiable heat signature. We formulate a three-stage taxonomy separating reversible premeasurement, irreversible record formation, and memory reset, and derive a conditional record-formation heat bound: under explicit operational conditions (C1 to C6) in the uncontrolled-decoherence regime (no work extraction/coherence-recovery channel), the irreversible record-formation channel must dissipate at least $k_B T \ln 2$ of heat per bit of classical information created, quantified by the mutual information $I(X;Y)$ between a prepared classical label X and the recorded outcome Y. Using an explicit system/pointer/bath model, we identify the precise stage at which this Landauer cost is paid: not during unitary premeasurement coupling, but during irreversible environmental coupling, when the pointer becomes entangled with $N \gg 1$ environmental degrees of freedom and the record is stabilized. We design a circuit-QED differential microcalorimetry experiment using superconducting qubits and nanocalorimeters (TES or SNS nanobolometer class). The protocol employs matched ON/OFF branches that share identical premeasurement pulses and routing losses, differing only in whether an objective record is stabilized. The measurand is the per-shot differential deposited energy $\Delta Q \equiv Q_{\mathrm{ON}} - Q_{\mathrm{OFF}}$, which isolates the record-formation contribution. Four primary controls (ground-state baseline, measurement-strength scaling, reversal-delay timing sweep, and prior-variation) discriminate from systematic effects. Sensitivity analysis using demonstrated nanobolometer performance shows detection is feasible with $N \sim 2 \times 10^9$ to 8×10^9 ON/OFF pairs at 10 mK for Landauer-scale residual tests at SNR ~ 10 (for $\sigma_Q \approx 0.32$ to 0.6 zJ and $\Delta Q_{\mathrm{target}} \approx 9.57 \times 10^{-5}$ zJ). The bound is falsified if the observed residual $\Delta Q - k_B T \ln 2 \cdot I(X;Y)$ falls statistically below zero.

Keywords: quantum measurement; Landauer principle; thermodynamics of information; objective classical record; record formation; mutual information; decoherence; quantum Darwinism; circuit QED; superconducting qubits; differential microcalorimetry; nanocalorimetry

1. Introduction

The quantum measurement problem concerns how definite outcomes emerge from quantum superpositions. We propose a thermodynamic resolution: the formation of an *objective classical record* is a physical event that converts quantum uncertainty into classical certainty with a thermodynamic resource cost that becomes a dissipative floor only under explicit operational conditions.

This cost is not merely conceptual. Landauer's principle establishes that any logically irreversible operation erasing one bit of information must dissipate at least $k_B T \ln 2$ of heat [1]. We hypothesize that irreversible record formation in quantum measurement is such an operation: stabilizing a classical record eliminates quantum alternatives and exports entropy to the environment. This paper formulates the hypothesis as a conditional, falsifiable bound and designs an experiment to test it.

However, applying Landauer's principle to quantum measurement has generated controversy. Critics argue that: (i) the principle applies to erasure, not measurement [3]; (ii) measurement can be

 doi:10.20944/preprints202602.1739.v1

performed reversibly with no heat cost [2]; and (iii) any "Landauer cost" can be deferred indefinitely to memory reset [2].

We resolve these tensions by providing a precise taxonomy of measurement stages and identifying exactly where the Landauer bound applies. Our claim is not that "measurement" in general costs $k_B T \ln 2$ per bit. Rather, the bound is a conditional statement about *record formation* in a thermal environment with a classical register and a cyclic apparatus.

Recent theoretical work supports this connection. Cortês and Liddle showed that Hawking evaporation saturates the Landauer bound [6], a result extended in a companion work to a complete thermodynamic cycle of information creation and destruction [20]. Together these results motivate the possibility that Landauer-scale thermodynamics constrains fundamental physical processes beyond classical computing. Latune and Elouard analyzed thermodynamic costs of measurement apparatus, showing that measurements *can* approach reversibility when no stable record is created [9]. Mohammady and Buscemi identified a "thermodynamic trilemma" constraining efficient measurements [10]. Touil *et al.* formalized objective record formation through quantum Darwinism, where classical objectivity emerges via redundant environmental encoding [8].

Our contribution is threefold:

1. A three-stage taxonomy cleanly separating reversible correlation, record formation, and reset, with explicit operational conditions
2. A **record-formation heat bound** expressed in terms of measurable classical mutual information $I(X;Y)$
3. A falsifiable differential microcalorimetry experiment with quantitative sensitivity analysis and a complete calibration/systematics program

 doi:10.20944/preprints202602.1739.v1

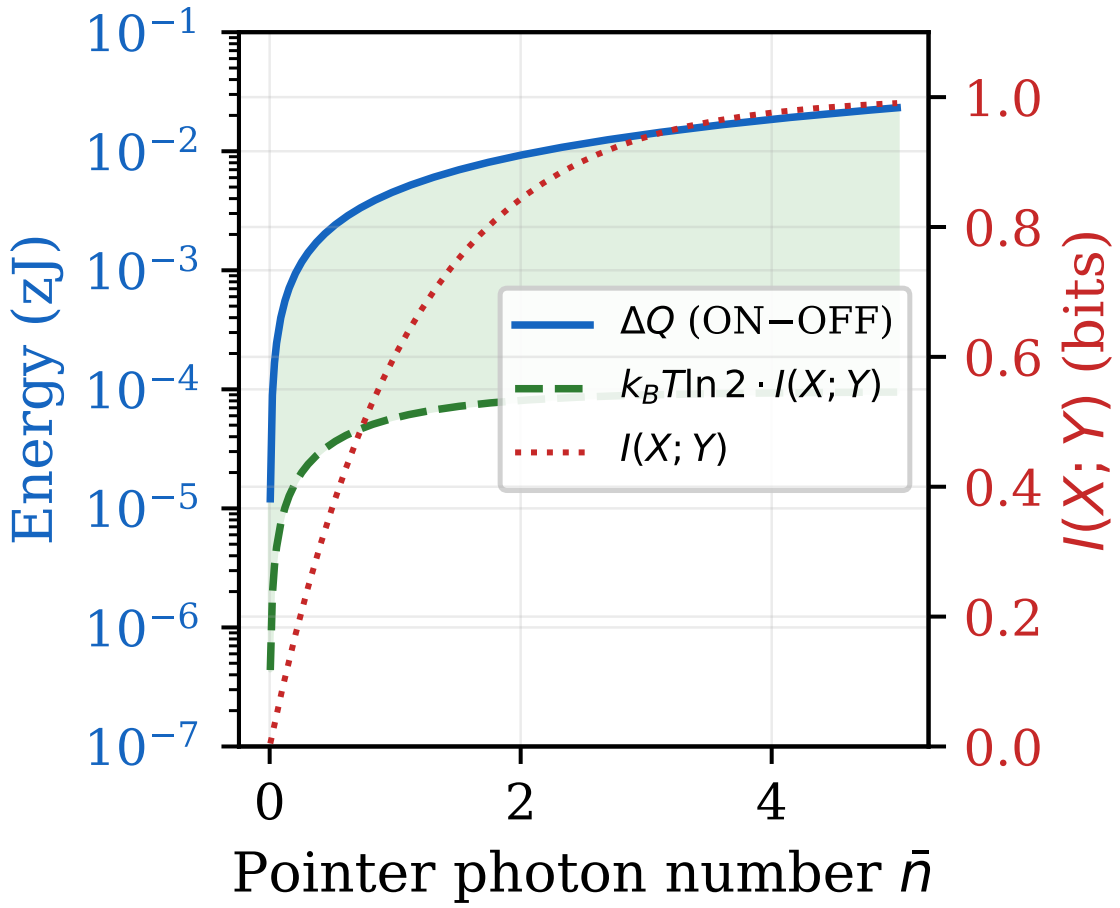

Figure 1. Predicted differential heat ΔQ (solid blue, left axis) and Landauer bound $k_B T \ln 2 \cdot I(X;Y)$ (dashed green, left axis) versus pointer photon number $\bar{n}$, at $T = 10$ mK with uniform prior $p(0) = p(1) = 1/2$. The shaded region shows the positive residual $\Delta Q - k_B T \ln 2 \cdot I(X;Y) > 0$ at all tested measurement strengths. The dotted red curve (right axis) shows the classical mutual information $I(X;Y)$ rising from 0 to 1 bit as $\bar{n}$ increases. In the deep-quantum regime ($\bar{n} \sim 1$), $\Delta Q \sim h\nu$ exceeds the bound by $\sim 48\times$; near-saturation tests require pointer energies closer to $k_B T \ln 2$.

2. Three-Stage Taxonomy and Operational Definitions

2.1. Stages: Premeasurement, Record Formation, Reset

We decompose quantum measurement into three analytically distinct stages. This is a conceptual framework for identifying where the Landauer cost is paid; the measurement event itself is Stage 2.

1. **Stage 1: Reversible premeasurement (unitary correlation).** The system S becomes correlated/entangled with a pointer P via a unitary U_{SP}. No entropy production occurs. No Landauer cost. The pointer states $|P_i\rangle$ are distinguishable but the process can be unitarily reversed.
   Thermodynamic status: Thermodynamically reversible in principle; no Landauer cost in the ideal limit. (Real hardware produces residual dissipation from control pulses, but this is common-mode and cancels in the differential measurement.)
   Information status: Quantum correlations between S and P increase (the reduced states become mixed), but no classical record Y exists yet. The classical mutual information $I(X;Y)$ is not defined at this stage because no decohered outcome register has been created.
2. **Stage 2: Irreversible record formation (objective stabilization).** The pointer couples to a thermal bath, creating a macroscopic record via redundant environmental encoding ($N \gg 1$ environmental degrees of freedom). The record is stabilized against reversal. This stage is logically irreversible and is where Landauer-scale heat is paid.

 doi:10.20944/preprints202602.1739.v1

Thermodynamic status: Entropy flows to the bath. The bound applies here when conditions C1 to C6 hold.
Information status: Classical mutual information $I(X;Y)$ is created. The outcome Y becomes a definite classical variable.

3. **Stage 3: Reset (optional reusability).** Erasing the record to reuse the apparatus. Standard Landauer erasure cost. Reset can occur long after the measurement; it is conceptually distinct from record formation.
Thermodynamic status: Entropy flows to the bath during reset.
Information status: Classical information is destroyed.

This taxonomy resolves apparent contradictions: "reversible measurements" address Stage 1 (and possibly engineered avoidance of Stage 2), while Landauer bounds constrain Stage 2 when an objective record is actually created. The "cost can be deferred to reset" objection addresses Stage 3 rather than Stage 2.

2.2. Operational Definition: Objective Record Formation

Let X be a classical random variable labeling the prepared input and Y be the classical outcome stored in a record register. We call Y an **objective record** if, operationally:

1. **Stability:** Y persists for time $t \gg \tau_c$, where τ_c is the reversibility time beyond which a coherent reversal operation fails to recover the initial state fidelity (defined precisely in Sec. 12).
2. **Classical definiteness:** The record is well-approximated by a classical register with negligible coherence between distinct outcomes in the record basis.
3. **Redundancy (strengthening criterion):** Following quantum Darwinism [7,8], the outcome information is redundantly encoded in environmental degrees of freedom. Quantitatively, the accessible information I^F_{acc} between the system variable X and an environmental fragment F satisfies
$$\frac{I^F_{\text{acc}}}{H(X)} \geq 1 - \delta \quad \text{for} \quad f \leq f_0, \tag{1}$$
with fragment fraction f and small δ (e.g., $\delta \sim 0.1$), giving redundancy $R \approx 1/f_0$. (This criterion provides theoretical grounding from quantum Darwinism; the proposed experiment does not directly measure the fragment-information curve but tests the thermodynamic consequence.)

Our thermodynamic criterion: **measurement occurs when this irreversible encoding dissipates heat**. Objectivity is asserted when the redundancy plateau coincides with $\tau > \tau_c$ and the calorimetric signature exceeds the 3σ detection criterion.

3. Record-Formation Heat Bound

3.1. General Inequality

We model record formation as a completely positive trace-preserving (CPTP) map $\mathcal{E}$ that (i) produces a classical register Y with statistics $p(y|x)$ and (ii) couples irreversibly to a thermal bath at temperature T. From the generalized second law for information processing [5], the entropy production Σ satisfies
$$\Sigma = \beta\langle Q_{\text{rec}}\rangle + \Delta S_{\text{sys}} + \Delta S_{\text{mem}} - I^{\text{gain}}_{S:M} \geq 0, \tag{2}$$
where ΔS_{sys} is the entropy change of the measured system S, ΔS_{mem} is the entropy change of *reusable* apparatus degrees of freedom kept inside the Stage 2 system boundary (pointer/control modes reset between trials), and $I^{\text{gain}}_{S:M}$ is the mutual information gained between S and the memory M. In this bookkeeping, the stabilized macroscopic record in the absorber/environment is treated on the bath side of the channel, so its irreversible entropy production contributes to $\beta\langle Q_{\text{rec}}\rangle$ rather than to ΔS_{mem}. In the experiment, the measured classical quantity $I(X;Y) = I(X;Y)$ is used as a conservative lower bound on this gain. We take an initially thermal bath so that the bath-entropy term is $\beta\langle Q_{\text{rec}}\rangle$. Throughout,

 doi:10.20944/preprints202602.1739.v1

entropy terms (ΔS and $I_{S:M}^{\text{gain}}$) are dimensionless (nats, i.e., in units of k_B), and information quantities ($I(X;Y)$) are in bits. The factor $\ln 2$ converts between them: 1 bit $= \ln 2$ nats. In natural units,

$$\beta\langle Q_{\text{rec}}\rangle \geq (\ln 2)\, I(X;Y) - \Delta S_{\text{sys}} - \Delta S_{\text{mem}}, \tag{3}$$

with $\beta = 1/(k_B T)$. This is a channel-level inequality for the Stage 2 map under the stated bookkeeping boundary, not a universal standalone theorem for arbitrary measurement implementations.

3.2. Conditional Bound (Corollary)

If, during Stage 2, a classical record is created via irreversible entropy export to the bath (redundancy generation), and if the reusable apparatus degrees included in ΔS_{mem} are cycled back to a reference state over each ON/OFF trial (so net $\Delta S_{\text{mem}} \approx 0$), with $\Delta S_{\text{sys}} \approx 0$ and $W \approx 0$ for the record-formation channel, then:

$$\boxed{\langle Q_{\text{rec}}\rangle \geq k_B T \ln 2 \cdot I(X;Y)} \tag{4}$$

where

$$\begin{aligned} I(X;Y) &= H(Y) - H(Y|X) \\ &= \sum_{x,y} p(x)\, p(y|x)\, \log_2 \frac{p(y|x)}{\sum_{x'} p(x')p(y|x')}. \end{aligned} \tag{5}$$

For an ideal binary projective measurement with uniform prior $p(X{=}0) = p(X{=}1) = 1/2$, this gives $I(X;Y) = 1$ bit. Here Y denotes the classical ON-branch record variable, defined operationally as the binary macrostate of the absorber: a thresholded temperature excursion ΔT above or below a discriminator level, corresponding to pointer-conditioned thermalization. This absorber macrostate is the physical record created in Stage 2; it is the degree of freedom whose creation costs heat.

In production calorimetry we do not perform shot-resolved outcome readout of Y; instead $I(X;Y)$ is obtained from *separate* dispersive calibration blocks (not interleaved with calorimetric acquisition) using identical premeasurement pulses to infer $p(x)$ and $p(y|x)$. Because the dispersive readout and absorber thermalization both respond to the same pointer displacement (the qubit-state-conditioned coherent state $|\alpha_\sigma\rangle$), they share the same state-dependent distinguishability: a qubit state that produces a large pointer displacement yields both a high-confidence dispersive outcome *and* a large absorber temperature excursion. This substitution is accepted only after branch-matching tests and state-conditioned absorber histograms verify that the ON-branch pointer populations are consistent with the calibrated confusion matrix within uncertainty; otherwise the run is rejected for bound testing. If ΔS_{sys} or ΔS_{mem} is non-negligible, or if external work W is supplied, the full bound reads

$$\langle Q_{\text{rec}}\rangle \geq k_B T \ln 2 \cdot I(X;Y) - k_B T \Delta S_{\text{sys}} - k_B T \Delta S_{\text{mem}} - W, \tag{6}$$

where $W \geq 0$ is work supplied to the apparatus by an external agent during Stage 2 (if any). We design the protocol to minimize these correction terms (cyclic apparatus, no external work). The quantity $I(X;Y)$ is a conservative (lower-bound) estimator of the thermodynamic information created because the actual record may contain additional correlations with unmonitored environmental degrees of freedom, so the true information gain $I_{S:M}^{\text{gain}} \geq I(X;Y)$. Equation (4) is therefore a conditional operational statement for the Stage 2 channel under C1 to C6, not a universal claim for arbitrary measurement decompositions. Protocols that keep the pointer coherent and defer entropy export fall into the cost-shifting classes of Sec. 4, where dissipation can move to later readout/reset.

Interpretation of Stage 2 versus Stage 3 bookkeeping. The generalized second law bounds entropy production for each irreversible channel. Equation (4) is written for the Stage 2 channel under our boundary choice: reusable pointer/control modes are internal and cycled ($\Delta S_{\text{mem}} \approx 0$ under C3), while the stabilized macroscopic record is bath-side. Under that bookkeeping, entropy exported to the bath during record stabilization contributes to $\beta\langle Q_{\text{rec}}\rangle$ in Stage 2. If Stage 3 later erases a stored record,

 doi:10.20944/preprints202602.1739.v1

it typically incurs further dissipation; however, the exact Stage 2/Stage 3 split in a full-cycle budget is protocol-dependent and must be evaluated with explicit state accounting.

The temperature T is the effective temperature of the dissipative degrees of freedom that stabilize the record (Stage 2), calibrated in situ on the absorber/bath node.

3.3. Operational Conditions (C1 to C6)

The bound is asserted as a *conditional* statement:

C1 A thermal bath at temperature T is present during Stage 2.

C2 A classical register Y is created (decohered pointer with redundant environmental encoding).

C3 The apparatus begins in a standard state and is cyclic over Stage 2, or its entropy change is explicitly accounted.

C4 Irreversibility arises from bath coupling: no reversal operation that includes the bath degrees of freedom is performed on the experiment timescale. This is the operational definition of "objective": the record persists because reversing it would require controlling the bath.

C5 No unaccounted work reservoir supplies free energy; if work is supplied, the inequality includes the work term.

C6 $I(X;Y)$ is the actual classical mutual information for the chosen measurement strength.

What the bound does not imply:

- Measurement *in general* always costs $k_B T \ln 2$ per bit.
- Heat dissipation alone proves objectivity.
- All entropy production in a measurement protocol is due to Landauer cost.

4. When the Bound Does Not Apply (or Is Shifted)

We distinguish four non-applicability and cost-shifting classes:

A. **Premeasurement only.** If the pointer is captured before environmental coupling (Stage 1 only), no record is formed and no Landauer cost is incurred. This is the regime of reversible measurement protocols [11]. Coherence can be recovered by applying the inverse unitary.

B. **Deferred record in quantum memory.** If the pointer state is stored coherently without thermalization, no classical record exists and the cost is deferred until readout or reset. This is not free: maintaining coherence over time is a resource cost that scales with storage duration.

C. **Fresh memory or work-assisted recording.** If a low-entropy memory is consumed or external work supplies free energy, the heat released to the bath can be reduced. The cost is shifted into memory entropy or work, not eliminated.

D. **Weak or zero-information regimes.** When $I(X;Y) < 1$, the bound scales proportionally. For constant preparation with $I(X;Y) = 0$, the predicted heat is zero within experimental noise.

4.1. Reconciliation with Reversible Measurement Protocols

Latune and Elouard [9] analyze thermodynamically optimal measurement protocols and show that measurement can approach reversibility. This is **compatible** with our framework:

1. Their "reversible" protocols operate in Stage 1 (premeasurement).
2. No objective classical record is created in the reversible limit.
3. If an objective record is eventually created, the Landauer cost is paid.

The key distinction: **correlation** (Stage 1) is reversible; **record formation** (Stage 2) is not.

This mapping is also consistent with Bennett's reversible computation arguments [2]: premeasurement is analogous to reversible computation; record formation is analogous to writing output to a permanent register. The Landauer cost is paid when you commit to a permanent record.

 doi:10.20944/preprints202602.1739.v1

4.2. Addressing Norton's "Waiting for Landauer"

Norton [3] argues that Landauer's principle is not universally applicable. We agree with Norton's caution, and respond (following the defense by Ladyman and Robertson [4]) by specifying the operational conditions under which it applies:

- **Does apply**: Record formation with entropy flow to the bath (Stage 2), when conditions C1 to C6 hold.
- **Does not apply**: Reversible premeasurement (Stage 1).
- **Does not apply**: Quantum correlations that are never stabilized as classical records.

4.3. Work vs. Heat Classification of Pointer Absorption

A natural objection is that the pointer photon arrives as a coherent microwave pulse, directed energy that might be classified as *work* rather than heat, trivially satisfying the bound. We address this as follows.

The work term W in condition C5 refers to free energy supplied by an external agent to *drive* the record-formation process (e.g., a work reservoir that lowers the thermodynamic barrier to stabilization). In our protocol, no such external work is supplied: the pointer-absorber coupling is passive, and thermalization occurs spontaneously. The pointer photon's energy is the *input* to Stage 2, the physical carrier of information, not work done *on* the record-formation channel.

Upon absorption, the photon's energy is distributed among $N \gg 1$ electron-phonon degrees of freedom in the absorber at temperature T. After thermalization, the energy cannot be extracted as work without additional information about the absorber's microstate. This irreversible thermalization *is* the record-formation process: it converts a low-entropy coherent state (the pointer) into a high-entropy thermal state (the absorber macrostate), creating the classical record. The deposited energy therefore satisfies the thermodynamic definition of heat: stochastic energy transfer from the system to a thermal reservoir, increasing the reservoir's entropy.

The experimental controls provide an independent check: the toggle-only and pointer-disabled null protocols (Sec. 13) bound any residual work-like contributions from control lines and switching operations. Any ON/OFF asymmetry from these sources enters the systematic budget (Table 2) and is subtracted before residual analysis.

5. Explicit Model: Where the Landauer Cost Is Paid

Having specified the operational regime and its boundaries, we now construct a concrete system/pointer/bath model to identify the precise microscopic origin of the heat flow.

5.1. The model: System + Pointer + Bath

Consider a spin-1/2 system in superposition:

$$|\psi_S\rangle = \alpha|\uparrow\rangle + \beta|\downarrow\rangle, \quad |\alpha|^2 + |\beta|^2 = 1. \tag{7}$$

The apparatus consists of a pointer degree of freedom P (initially in state $|P_0\rangle$, e.g., a resonator mode) and a thermal environment at temperature T with many degrees of freedom E, initially in $\rho_E^{\text{th}} \propto e^{-H_E/(k_B T)}$. For compactness, the ket notation below uses $|E_0\rangle$ as a representative purification/microstate of this thermal ensemble.

5.2. Stage 1: Premeasurement (Reversible)

Unitary system/pointer coupling:

$$\big(\alpha|\uparrow\rangle + \beta|\downarrow\rangle\big)|P_0\rangle \xrightarrow{U_{SP}} \alpha|\uparrow\rangle|P_\uparrow\rangle + \beta|\downarrow\rangle|P_\downarrow\rangle. \tag{8}$$

This process is thermodynamically reversible in principle. The pointer states are correlated but no entropy has been exported to the environment. This is *not* record formation.

 doi:10.20944/preprints202602.1739.v1

5.3. Stage 2: Record Formation (Irreversible; Landauer Cost Paid)

The pointer couples to the thermal bath, creating redundant environmental copies:

$$\begin{aligned} &\alpha|\uparrow\rangle|P_\uparrow\rangle|E_0\rangle + \beta|\downarrow\rangle|P_\downarrow\rangle|E_0\rangle \\ &\xrightarrow{\text{spread}} \alpha|\uparrow\rangle|P_\uparrow\rangle|E_\uparrow^{(N)}\rangle + \beta|\downarrow\rangle|P_\downarrow\rangle|E_\downarrow^{(N)}\rangle, \end{aligned} \tag{9}$$

where $|E_\sigma^{(N)}\rangle$ represents $N \gg 1$ environmental degrees of freedom encoding outcome σ. The environmental states satisfy:

$$\langle E_\uparrow^{(N)}|E_\downarrow^{(N)}\rangle \approx e^{-N/N_c} \to 0 \quad \text{for } N > N_c. \tag{10}$$

In the operational regime C1 to C6, we hypothesize that this environmental coupling is where a Landauer-scale thermodynamic cost is incurred. The physical basis: the redundant environmental encoding is an irreversible entropy export; reversing it would require controlled access to all N bath degrees of freedom, which is operationally excluded by C4. Under the generalized second law (Sec. 3), this irreversible entropy production implies $Q \geq k_B T \ln 2$ per bit of classical information stabilized. The proposed experiment tests whether this cost is detectable as a calorimetric signature.

Eq. (4) is therefore a lower bound for the first logical bit in this open-system regime; in this model family, additional redundancy generally increases total entropy export to the environment, though exact scaling is protocol-dependent.

5.4. Identification of the Record-Formation Information

After Stage 2, tracing over the environment gives the reduced state:

$$\rho_{SP}^{\text{final}} = |\alpha|^2|\uparrow\rangle\langle\uparrow| \otimes |P_\uparrow\rangle\langle P_\uparrow| + |\beta|^2|\downarrow\rangle\langle\downarrow| \otimes |P_\downarrow\rangle\langle P_\downarrow|. \tag{11}$$

The classical information created in the record is (in bits):

$$H(Y) = H(|\alpha|^2) = -|\alpha|^2 \log_2 |\alpha|^2 - |\beta|^2 \log_2 |\beta|^2. \tag{12}$$

For equal superposition ($|\alpha|^2 = |\beta|^2 = 1/2$), $H(Y) = 1$ bit. This single-state expression is the record-outcome entropy. The experimental bound variable remains $I(X;Y) = I(X;Y)$, where X is the prepared classical label (Sec. 2.2).

The quantitative heat bound $Q \geq k_B T \ln 2 \cdot I(X;Y)$ follows from the generalized second law (Sec. 3), applied to this model with $I_{S:M}^{\text{gain}} \geq I(X;Y)$. The model identifies the *physical mechanism*: record formation occurs when the pointer-environment overlap $\langle E_\uparrow^{(N)}|E_\downarrow^{(N)}\rangle$ drops below the reversal criterion, and the resulting entropy flow to the environment carries the Landauer cost. For 1 bit: $Q \geq k_B T \ln 2$.

5.5. Lindblad Master Equation Validation

To bridge the gap between the analytical model and the proposed experiment, we solve the Lindblad master equation for a qubit-resonator system with parameters matching the experimental architecture [18].

Model. A transmon qubit (two-level, $T_1 = T_2 = 50\ \mu$s) dispersively coupled ($\chi/2\pi = 2$ MHz) to a resonator ($\omega_r/2\pi = 7$ GHz). The post-premeasurement state is

$$|\psi_{\text{PM}}\rangle = \tfrac{1}{\sqrt{2}}\big(|0\rangle|\alpha\rangle + |1\rangle|-\alpha\rangle\big), \tag{13}$$

with $|\alpha|^2 = \bar{n} = 1$, representing Stage 1 completion. Two Stage 2 branches are simulated independently:

- **ON branch**: the resonator decays into the absorber with $\kappa_{\text{ON}}/2\pi = 5$ MHz (fast thermalization).
- **OFF branch**: the pointer is held in a storage cavity with $\mathcal{Q}_{\text{storage}} = 5 \times 10^7$ ($\kappa_{\text{OFF}}/2\pi \approx 140$ Hz), and an ideal reversal (controlled displacement) is applied after delay τ_d.

 doi:10.20944/preprints202602.1739.v1

ON branch results (Fig. 2). The resonator photon number decays from $\bar{n} = 1$ to zero within $\sim 0.5\ \mu$s. The cumulative heat deposited in the bath reaches $Q_{\text{bath}} = \hbar\omega_r \approx 4.64 \times 10^{-3}$ zJ, equal to the pointer photon energy $h\nu$ and exceeding $k_B T \ln 2$ by a factor of ~ 48. The qubit's von Neumann entropy rises from near zero to ~ 1 bit as the resonator decay transfers which-path information irreversibly to the bath. The qubit off-diagonal element $|\rho_{01}|$ simultaneously decays, reflecting the loss of quantum coherence during record stabilization. These dynamics confirm that the Landauer bound $Q \geq k_B T \ln 2 \cdot I(X;Y)$ is satisfied (with large positive residual) in the deep-quantum operating regime.

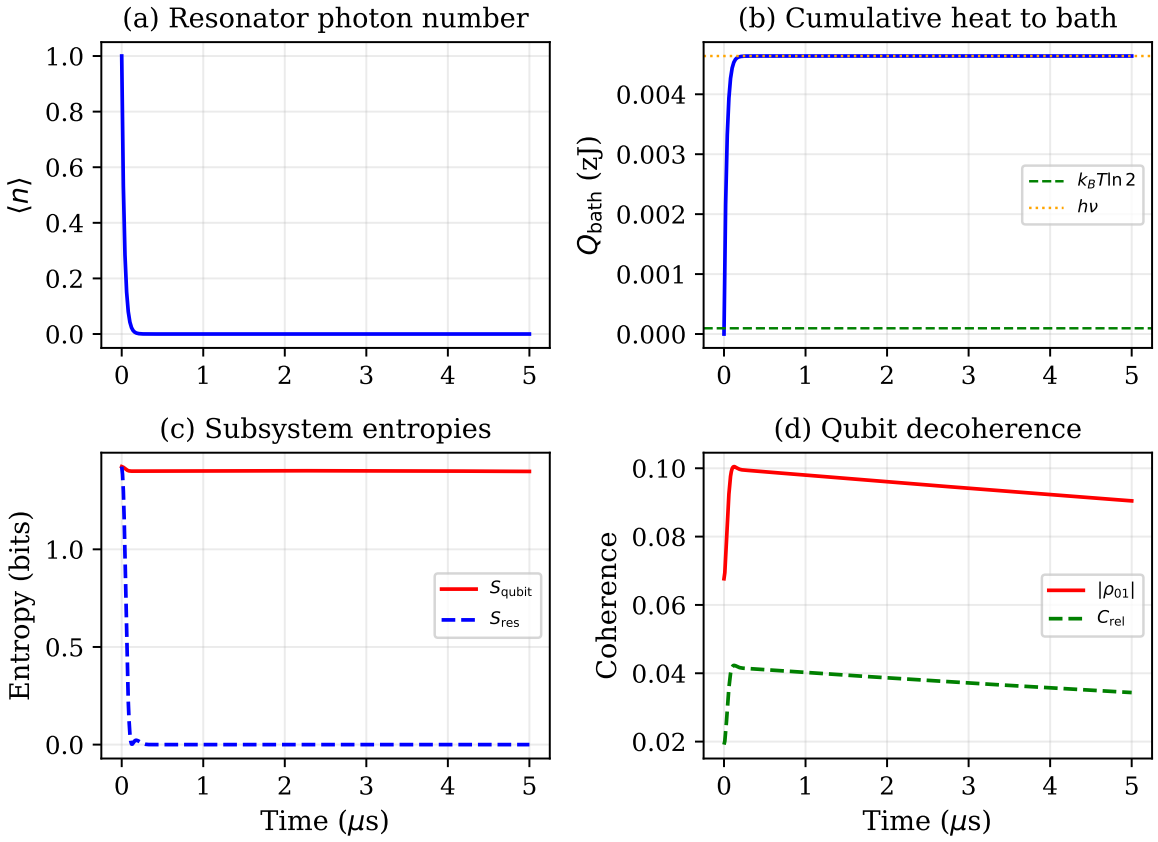

Figure 2. Lindblad simulation of the ON branch (record formation). (a) Resonator photon number decaying into the absorber ($\kappa_{\text{ON}}/2\pi = 5$ MHz). (b) Cumulative heat $Q_{\text{bath}} = \hbar\omega_r(\bar{n}_0 - \bar{n}(t))$ reaching $h\nu \approx 4.64 \times 10^{-3}$ zJ, far above the Landauer floor $k_B T \ln 2 \approx 9.57 \times 10^{-5}$ zJ. (c) Subsystem entropies: qubit entropy rises to ~ 1 bit; resonator entropy peaks during decay and returns to zero. (d) Qubit off-diagonal $|\rho_{01}|$ and relative entropy of coherence C_{rel} during decoherence. Parameters: $\bar{n} = 1$, $\chi/2\pi = 2$ MHz, $T = 10$ mK, $T_1 = T_2 = 50\ \mu$s.

OFF branch and τ_c extraction (Fig. 3). A reversal delay sweep determines the reversibility time τ_c. At each delay τ_d, the premeasurement state evolves with the storage-cavity decay rate, then a time-dependent controlled displacement (accounting for the dispersive phase rotation) returns the resonator to vacuum. The recovery fidelity $\mathcal{F}(\tau_d) = \langle\psi_0|\rho_{\text{rev}}|\psi_0\rangle$ is computed against the initial (pre-premeasurement) state.

The fidelity remains above 0.99 for $\tau_d < 100$ ns, providing $\approx 78\times$ margin over the catch-and-release reversal window. Fidelity drops below 0.9 at $\tau_c \approx 8\ \mu$s, driven primarily by qubit T_2 decoherence and slow photon leakage from the storage cavity. This is consistent with (and slightly below) the order-of-magnitude estimate $\tau_c \sim 10$ to $50\ \mu$s in Sec. 12.

 doi:10.20944/preprints202602.1739.v1

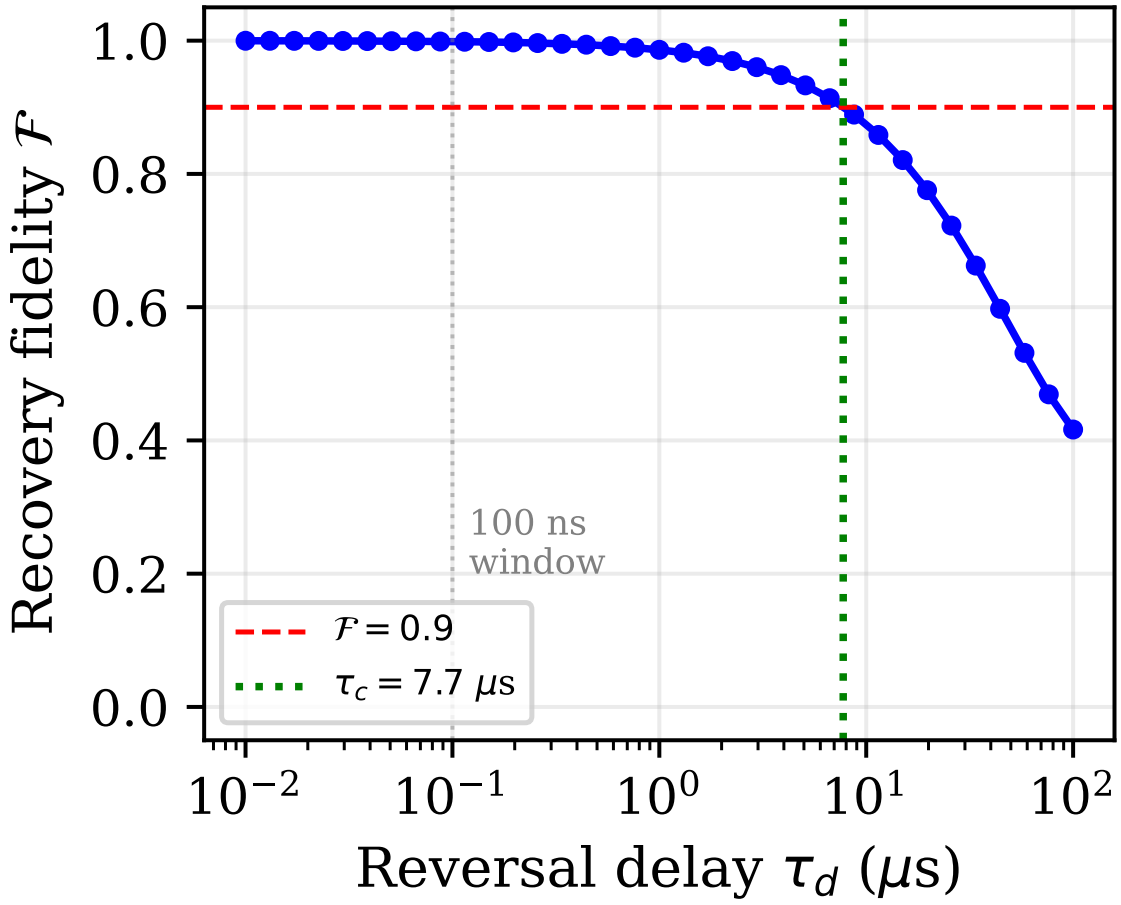

Figure 3. OFF-branch reversal fidelity versus delay τ_d. The fidelity remains near unity for $\tau_d \lesssim 1$ μs and drops below 0.9 at $\tau_c \approx 8$ μs (green dashed line), providing $\approx 78\times$ margin over the 100 ns reversal window (gray dotted line). Storage cavity $Q = 5 \times 10^7$; qubit $T_1 = T_2 = 50$ μs.

Model limitations. The simulation uses a Markovian bath (Lindblad), finite Fock-space truncation ($N = 10$), and an idealized controlled-displacement reversal. The premeasurement state is prepared directly rather than simulated through an explicit drive pulse. The reversal accounts for the dispersive phase rotation but uses a known-amplitude displacement, which is more idealized than the experimental echo protocol. Consequently, the simulated τ_c is an upper bound on the experimentally achievable reversibility time.

6. Experimental Architecture

6.1. Platform and Setup

- **System**: Superconducting transmon qubit ($\omega_q/2\pi \sim 5$ GHz)
- **Readout**: Dispersive measurement via coupled resonator
- **Calorimeter**: On-chip nanocalorimeter (TES or SNS nanobolometer class) in thermal contact with the record-formation channel (not the amplifier chain)
- **Environment**: Dilution refrigerator; $T \approx 10$ mK is the measured effective temperature of the record-formation absorber, calibrated in situ

Thermal-detector qubit readout has been demonstrated with single-shot fidelity and microsecond durations [12], establishing platform feasibility.

 doi:10.20944/preprints202602.1739.v1

6.2. The ON/OFF Toggle Architecture

The core design element is a **hardware toggle** that routes the pointer mode to different fates while keeping all other dissipation channels identical.

6.2.1. Common Path (Both Branches)

1. A classical random number generator selects a preparation label $x \in \{0, 1, \ldots\}$ according to the prior $p(x)$. The qubit is then prepared in the corresponding state $|\psi_x\rangle$ (e.g., $|\psi_0\rangle = |0\rangle$, $|\psi_1\rangle = |+\rangle$). The label x is the classical variable X that enters $I(X;Y)$.
2. Apply dispersive readout pulse (identical timing, amplitude, frequency).
3. Qubit-resonator entanglement creates pointer state (premeasurement).

6.2.2. Branch Point: Three-Port Tunable Coupler

A flux-biased three-port tunable coupler (e.g., transformer SQUID device [16,17]) routes the pointer mode to different fates while keeping upstream conditions identical. The coupler must satisfy:

- **Amplitude/phase matching**: identical transfer function in both states
- **Isolation**: ≥ 40 dB between ON and OFF paths to limit leakage
- **Low added dissipation**: routing loss $\ll \Delta Q$ per shot; switching within a few ns. The switch is thermally anchored to the bath and spatially isolated from the calorimeter to ensure control-pulse dissipation does not couple to the sensor.
- **Characterization**: verified by injected calibration pulses upstream

6.2.3. ON Branch: Record Formation

The on-chip absorber (AuPd thin-film resistor or SNS junction) has a dual role: it is both the *record register* (where the pointer photon is thermalized into $N \gg 1$ electron and phonon degrees of freedom, creating the objective record) and the *calorimetric sensor* (whose temperature rise is the measured signal). The calorimeter therefore directly couples to the physical location where the record is formed, not to a downstream amplifier chain.

1. Pointer mode absorbed by the on-chip absorber.
2. Thermalization creates the macroscopic record in the absorber's internal degrees of freedom ($N \gg 1$ environmental DOF).
3. Heat deposited in calorimeter: $Q_{\mathrm{ON}} = Q_{\mathrm{cm}} + Q_{\mathrm{rec}}$.

6.2.4. OFF Branch: Coherent Reversal

The coupler must route the pointer into the storage cavity before the pointer has time to couple to uncontrolled environmental modes (stray radiation, substrate phonons). The routing delay must satisfy $\tau_{\mathrm{route}} \ll \tau_c$, where τ_c is the record-formation timescale. For typical dispersive readout, the pointer is a coherent state in a well-isolated resonator mode, and the routing can complete in a few ns, well before environmental coupling becomes significant.

1. The pointer mode is adiabatically captured in a high-$\mathcal{Q}$ storage cavity ($\mathcal{Q} \sim 5 \times 10^7$, with minimum acceptable $\mathcal{Q} > 10^7$) via the tunable coupler. Transfer leakage must satisfy $\delta Q_{\mathrm{transfer}} < 0.1 \cdot k_B T \ln 2$, i.e., $< 9.57 \times 10^{-6}$ zJ at 10 mK. For a single-photon pointer ($E_\gamma \approx 4.64 \times 10^{-3}$ zJ at 7 GHz), this requires capture efficiency $> 99.8\%$, consistent with demonstrated catch-and-release protocols [16].
2. A measurement reversal pulse sequence is applied [11]: by reversing the dispersive interaction (through qubit echo or opposite-phase drive), the qubit-pointer entanglement is erased. This uncomputation must complete within the pointer's coherence time. For transmon qubits with $T_2 \gtrsim 50$ μs, a < 100 ns echo sequence is consistent with demonstrated weak-measurement reversal timescales [11].
3. The qubit's coherence is fully restored with high fidelity ($\mathcal{F} > 0.9$), and the storage cavity returns to vacuum.

 doi:10.20944/preprints202602.1739.v1

4. No classical outcome is recorded; ideally no net heat is generated: $Q_{\mathrm{OFF}} = Q_{\mathrm{cm}} + \delta Q_{\mathrm{leak}}$, with $\delta Q_{\mathrm{leak}} \ll Q_{\mathrm{rec}}$.

6.3. Measurand and Differential Estimator

The primary observable is the **differential heat**:

$$\Delta Q \equiv \langle Q \rangle_{\mathrm{ON}} - \langle Q \rangle_{\mathrm{OFF}}. \tag{14}$$

A minimal branch decomposition gives:

$$Q_{\mathrm{ON}} = Q_{\mathrm{cm}} + Q_{\mathrm{rec}}, \tag{15}$$

$$Q_{\mathrm{OFF}} = Q_{\mathrm{cm}} + \delta Q_{\mathrm{leak}}, \tag{16}$$

where Q_{cm} is common-mode energy (control pulses, routing losses, switch-drive dissipation) shared by both branches, and δQ_{leak} is parasitic heat in the OFF branch (Sec. 8). Under successful matching and low leakage, $\langle \Delta Q \rangle \approx \langle Q_{\mathrm{rec}} \rangle - \langle \delta Q_{\mathrm{leak}} \rangle \approx \langle Q_{\mathrm{rec}} \rangle$.

Switch-drive dissipation (flux-pulse heating in bias lines, 50 Ω termination losses) is common-mode because both branches are toggled with identical control pulses. The toggle-only null (Sec. 13) verifies that any residual ON/OFF asymmetry from the switch drive is below the detection criterion.

This design suppresses common-mode backgrounds (drive dissipation, routing losses) that are identical in both branches. The OFF branch is not merely a different input state but an explicit *no-objective-record* implementation, isolating the thermodynamic cost of record formation from premeasurement correlation.

6.4. Shot timing and Experimental Sequence

1. **Initialize**: Reset qubit and resonator to ground state.
2. **Premeasurement**: Apply dispersive readout pulse to create pointer.
3. **Route**: Switch pointer to ON (absorber) or OFF (catch-and-release).
4. **Absorb/Capture**: ON branch thermalizes; OFF branch stores coherently.
5. **Reversal check (OFF)**: Uncompute and verify recovered-state fidelity.
6. **Thermal wait**: Allow calorimeter to relax or deconvolve overlapping pulses.

To avoid pile-up, choose $f_{\mathrm{rep}} \ll 1/\tau_{\mathrm{th}}$ or validate deconvolution for partially overlapping responses. Here f_{rep} denotes the ON/OFF *pair* repetition rate (pairs per second).

7. Thermal Circuit Model

7.1. Single-Node Model

We model the calorimeter as a single thermal node with heat capacity C and thermal conductance G to the bath. The thermal time constant is $\tau_{\mathrm{th}} = C/G$. For an impulse energy deposition Q at t_0, the temperature response is

$$\Delta T(t) = \frac{Q}{C}\, e^{-(t-t_0)/\tau_{\mathrm{th}}}\, \Theta(t - t_0), \tag{17}$$

with impulse response $h(t) = (1/C)\, e^{-t/\tau_{\mathrm{th}}} \Theta(t)$.

Using representative parameters at 10 mK:

$$C \approx 10^{-18}\ \mathrm{J/K} \quad \text{(AuPd absorber)}, \tag{18}$$

$$G \approx 10^{-12}\ \mathrm{W/K} \quad \text{(electron-phonon)}, \tag{19}$$

 doi:10.20944/preprints202602.1739.v1

giving $\tau_{\text{th}} \approx 1\ \mu$s (design target; demonstrated SNS devices achieve $\tau_{\text{th}} \sim 30\ \mu$s at comparable NEP [13]). The single-shot temperature rise for $Q_{\text{rec}} \approx 9.57 \times 10^{-5}$ zJ is

$$\Delta T \approx \frac{Q_{\text{rec}}}{C} \approx 0.1\ \mu\text{K} \quad (95.7\ \text{nK}). \tag{20}$$

To avoid attenuation of the lock-in response, choose $f_{\text{mod}} \ll 1/(2\pi\tau_{\text{th}})$.

7.2. Per-Shot Energy Estimator

Define a linear estimator using a weight function matched to the impulse response:

$$\hat{Q}_i = \int w(t - t_i)\, V_i(t)\, dt, \tag{21}$$

where $w(t)$ is the matched filter (optimal for stationary Gaussian noise) and $V_i(t)$ is the calorimeter voltage trace for shot i.

8. OFF-Branch Leakage Budget

Even in the OFF branch (no intentional dissipation), parasitic heat flows can occur. We enumerate all known sources and bound the total leakage δQ_{leak}.

Cavity photon decay.

The storage cavity has finite Q, so pointer photons leak as heat during storage. For a 7 GHz photon ($E_\gamma \approx 4.64 \times 10^{-3}$ zJ) in a cavity with $\mathcal{Q} = 5 \times 10^7$, the photon lifetime is $\tau_{\text{cav}} = \mathcal{Q}/\omega \approx 1.1$ ms. During a 100 ns reversal window, the fractional loss is $\sim 10^{-4}$, giving $\delta Q_{\text{cav}} \approx 4.1 \times 10^{-7}$ zJ per photon. This is the dominant leakage source but remains $\ll 9.57 \times 10^{-5}$ zJ.

Coupler isolation leakage.

The tunable coupler provides ≥ 40 dB isolation (10^{-4} power transmission). For a single-photon pointer ($E_\gamma \approx 4.64 \times 10^{-3}$ zJ), the leakage is $\delta Q_{\text{coupler}} \approx 4.64 \times 10^{-7}$ zJ.

Transfer leakage.

Imperfect capture into the storage cavity contributes $\delta Q_{\text{transfer}}$. The requirement from Sec. 6 is $\delta Q_{\text{transfer}} < 0.1 \cdot k_B T \ln 2 \approx 9.57 \times 10^{-6}$ zJ, corresponding to $> 99.8\%$ capture efficiency.

Quasiparticle generation.

Fast flux pulses can break Cooper pairs. Without mitigation, quasiparticle heating could reach $\sim 10^{-3}$ zJ per cycle. With well-shaped pulses and filtered bias lines (standard practice at 10 to 20 mK), quasiparticle generation is suppressed to $\delta Q_{\text{qp}} < 10^{-6}$ zJ per cycle.

Total leakage budget.

Summing the mitigated contributions:

$$\begin{aligned} \delta Q_{\text{leak}} &\approx \delta Q_{\text{cav}} + \delta Q_{\text{coupler}} + \delta Q_{\text{qp}} + \delta Q_{\text{transfer}} \\ &\lesssim 4.1 \times 10^{-7} + 4.64 \times 10^{-7} + 10^{-6} + 9.57 \times 10^{-6} \\ &< 1.12 \times 10^{-5}\ \text{zJ}, \end{aligned} \tag{22}$$

satisfying the requirement $\delta Q_{\text{leak}} < 0.15 \cdot \Delta Q_{\text{target}}$ for $\Delta Q_{\text{target}} \approx 9.57 \times 10^{-5}$ zJ. This budget assumes $\mathcal{Q} \sim 5 \times 10^7$ for the storage cavity (minimum acceptable $\mathcal{Q} > 10^7$), ≥ 40 dB coupler isolation, reversal completion within ~ 100 ns, and filtered bias lines for quasiparticle suppression. If coupler isolation degrades to 30 dB, the coupler leakage rises by $10\times$, reducing the safety margin. In-situ verification of isolation is therefore a go/no-go gate: the experiment should not proceed until the blocked-branch test (Sec. 11) confirms the required isolation.

 doi:10.20944/preprints202602.1739.v1

To keep OFF leakage below the Landauer scale, we require $(1-\mathcal{F})\,Q_{\text{pointer}} \ll k_B T \ln 2$. For a single-photon pointer ($Q_{\text{pointer}} \approx 4.64 \times 10^{-3}$ zJ), this requires $\mathcal{F} \gtrsim 0.98$. For $\bar{n} = 10$ photons ($Q_{\text{pointer}} \approx 4.64 \times 10^{-2}$ zJ), the requirement tightens to $\mathcal{F} \gtrsim 0.998$. Imperfect reversal ($\mathcal{F} < 1$) contributes an $\mathcal{O}(1-\mathcal{F})$ systematic at the Landauer scale, calibrated experimentally via Control 3 (Sec. 13).

9. Sensitivity Analysis

9.1. Energy Scales and the Quantum-Thermal Hierarchy

At $T = 10$ mK,

$$k_B T \ln 2 \approx 9.57 \times 10^{-26}\ \text{J} \approx 9.57 \times 10^{-5}\ \text{zJ}. \tag{23}$$

For comparison, a single 7 GHz readout photon carries $h\nu \approx 4.64 \times 10^{-24}$ J $\approx 48.5 \times k_B T \ln 2$.

This separation of scales ($h\nu \gg k_B T$) is advantageous for detection but requires careful interpretation. We distinguish

$$\Delta Q_{\text{signal}} \equiv \langle Q_{\text{ON}} - Q_{\text{OFF}} \rangle, \tag{24}$$

$$\Delta Q_{\text{bound}} \equiv k_B T \ln 2 \cdot I(X;Y). \tag{25}$$

In the deep-quantum operating point used here (typically $\bar{n} \sim 1$ at GHz frequencies), ΔQ_{signal} is expected to be dominated by pointer absorption ($\sim \bar{n} h\nu$) and therefore to lie well above ΔQ_{bound}. The primary falsification statistic is the residual $r = \Delta Q_{\text{signal}} - \Delta Q_{\text{bound}}$ after full leakage/systematics propagation; negative r at high significance would falsify the bound. Near-saturation tests (where r is not a priori large) require different operating points that reduce pointer-energy scale toward the Landauer scale (e.g., lower-frequency pointers or other low-energy platforms). In numerical validation, finite-sample Monte Carlo estimates of r can fluctuate below zero when per-shot noise dominates at low effective SNR; this does not constitute falsification. The experimental falsification criterion is a statistically significant negative residual after full uncertainty propagation (Sec. 13).

Control 4 (prior variation) is interpreted as a mechanism check at fixed pulse energy: it verifies how state populations modulate ΔQ_{signal}. By itself it does not isolate the Landauer floor; it constrains the state-dependent absorption model used in the residual analysis.

9.2. Detector Anchor

We anchor the feasibility estimate in the SNS nanobolometer of Kokkoniemi *et al.* [13] That platform has response times down to $\sim 30\ \mu$s at NEP ~ 60 zW$/\sqrt{\text{Hz}}$ and a predicted calorimetric energy resolution $\varepsilon \approx 0.32$ zJ when integrating up to the thermal cutoff frequency. Related calorimetric qubit-readout demonstrations motivate using this detector class as a realistic baseline [12,14].

9.3. Per-Shot Energy Uncertainty

For a calorimetric readout with effective bandwidth limited by τ_{th}, a conservative per-shot energy uncertainty may be taken as the reported calorimetric resolution:

$$\sigma_Q \sim \varepsilon \approx 3.2 \times 10^{-22}\ \text{J} \quad (0.32\ \text{zJ}). \tag{26}$$

A more conservative estimate uses $\sigma_Q = \text{NEP} \cdot \sqrt{\tau_m}$ with a shorter integration window τ_m, giving $\sigma_Q \approx 0.6$ zJ. We use $\sigma_Q = 0.32$ zJ for the primary shot-count estimate below; Table 1 presents the $\sigma_Q = 0.6$ zJ scenario to bound feasibility under less favorable conditions.

 doi:10.20944/preprints202602.1739.v1

9.4. Required Shot Count

Each differential measurement $\Delta Q_i = Q_{\mathrm{ON},i} - Q_{\mathrm{OFF},i}$ has per-shot variance $\sigma^2_{\Delta Q} = 2\sigma^2_Q$ (independent noise in both branches). For N independent ON/OFF pairs, the standard error of the mean is $\sigma_{\overline{\Delta Q}} = \sqrt{2}\,\sigma_Q/\sqrt{N}$. Targeting SNR $\equiv \langle \Delta Q \rangle / \sigma_{\overline{\Delta Q}}$ gives

$$N \gtrsim 2\left(\frac{\mathrm{SNR}\,\sigma_Q}{\Delta Q}\right)^2, \tag{27}$$

with $\Delta Q \sim h\nu \approx 4.64 \times 10^{-3}$ zJ (using the actual signal scale in the quantum regime, which is $\sim 48\times$ larger than the Landauer floor). At $T = 10$ mK and $\sigma_Q \approx 0.32$ zJ:

$$N_{\mathrm{SNR}=10} \sim 2\left(\frac{10 \times 0.32}{4.64 \times 10^{-3}}\right)^2 \approx 9.5 \times 10^5. \tag{28}$$

This is drastically more feasible than detecting the bare Landauer limit. However, to rigorously test the pointwise inequality near the much smaller $k_B T \ln 2$ floor (at 10 mK, $\sim 9.57 \times 10^{-5}$ zJ), the required averaging is much larger: $N \sim 2.24 \times 10^9$ for $\sigma_Q = 0.32$ zJ at SNR$=10$, or $N \sim 7.86 \times 10^9$ for $\sigma_Q = 0.6$ zJ (Table 1).

Table 1. Predicted signal and feasibility at SNR $= 10$ with $\sigma_Q = 0.6$ zJ (conservative, NEP-derived). t_{int} assumes 10^5 pairs/s (requires $\tau \lesssim 1$ μs); with demonstrated $\tau \sim 30$ μs bolometers, multiply by $\sim 100\times$.

T (mK)	$k_B T \ln 2$ (zJ)	N_{pairs}	t^*_{int}
10	9.57×10^{-5}	7.86×10^9	22 hours*
50	4.79×10^{-4}	3.14×10^8	52 minutes*
100	9.57×10^{-4}	7.86×10^7	13 minutes*

9.5. Integration Time Estimates

For $\tau_{\mathrm{th}} \sim 1$ μs (a design target not yet demonstrated), a repetition rate of $\sim 10^5$ pairs/s gives two distinct regimes: **(i)** for the full quantum-scale signal ($\Delta Q \sim h\nu$), $N_{\mathrm{SNR}=10} \sim 9.5 \times 10^5$ integrates in ~ 10 s; and **(ii)** for Landauer-scale resolution ($\Delta Q \sim 9.57 \times 10^{-5}$ zJ), integration is ~ 1.5 to 6 hours for SNR ~ 5 to 10 with $\sigma_Q = 0.32$ zJ, or ~ 22 hours for $\sigma_Q = 0.6$ zJ at SNR$=10$. Demonstrated SNS nanobolometers operate at $\tau_{\mathrm{th}} \sim 30$ μs [13]. In the lock-in regime with $f_{\mathrm{mod}} \sim 0.5$ to 5 kHz, the effective independent rate is typically a few kHz, stretching Landauer-scale integration to **days to weeks**. Faster bolometers or detector parallelization can recover hour-scale operation.

9.6. Temperature Regimes

Higher temperatures increase signal but also increase thermal noise; 10 mK represents the optimal trade-off for current detector technology. Two routes can reduce the required averaging: (i) operating at elevated effective temperature (increasing $k_B T \ln 2$ linearly), and (ii) increasing $I(X;Y)$ per cycle via multi-bit record creation.

 doi:10.20944/preprints202602.1739.v1

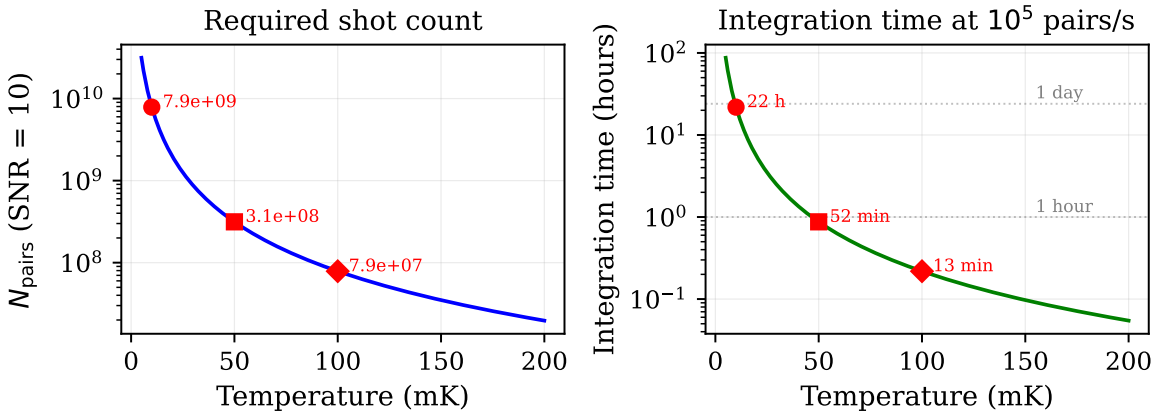

Figure 4. Temperature scaling of the Landauer-scale residual test ($\sigma_Q = 0.6$ zJ, SNR $= 10$, 10^5 pairs/s). Left: required ON/OFF pairs N. Right: integration time. Markers show the three operating points from Table 1. At 10 mK, integration requires ~ 22 hours with $\tau_{th} \lesssim 1$ μs bolometers; at 50 mK, ~ 52 minutes. With demonstrated $\tau_{th} \sim 30$ μs detectors, multiply times by $\sim 100\times$.

10. Lock-in Modulation Protocol

10.1. Modulation Scheme

Alternate ON/OFF branches at frequency f_{mod} chosen to lie above the $1/f$ noise corner (~ 10 Hz) and below the thermal cutoff $1/(2\pi\tau_{th})$. For the design target $\tau_{th} \sim 1$ μs, the cutoff is ~ 160 kHz and f_{mod} up to 5 kHz is comfortable. For demonstrated detectors with $\tau_{th} \sim 30$ μs, the cutoff is ~ 5.3 kHz, so $f_{mod} \lesssim 1$ kHz is appropriate.

The calorimeter voltage output is:

$$V(t) = V_{DC} + \mathcal{R}\,\Delta Q \cdot \cos(2\pi f_{mod} t) + n(t), \tag{29}$$

where $\mathcal{R}$ is the calorimeter responsivity (V/J) and V_{DC} is the common-mode baseline. Lock-in demodulation extracts $\mathcal{R}\,\Delta Q$ while rejecting:

- Common-mode V_{DC} (premeasurement + routing losses)
- Low-frequency drift
- Out-of-band noise

10.2. Power Modulation

For ON/OFF pair repetition rate f_{rep} (pairs/s) and square-wave alternation, the fundamental power modulation amplitude is

$$P_1 = \frac{2}{\pi}\,\Delta Q\, f_{rep}, \tag{30}$$

linking the lock-in output directly to ΔQ.

10.3. Drift and Stability Control

To suppress low-frequency drift, we employ:

- Lock-in modulation as above, extracting ΔQ from the demodulated response.
- Mixing chamber temperature stabilized via PID feedback to < 5 μK fluctuations at the modulation timescale.
- Periodic hardware null checks every 2 hours using the toggle-only and pointer-disabled protocols (Sec. 13).
- Allan deviation analysis of calibration pulse sequences to identify drift timescales.

 doi:10.20944/preprints202602.1739.v1

Data segments are accepted only if: (1) calibration pulse drift remains $< 0.1 \cdot \Delta Q_{\text{target}}$, (2) null checks yield ΔQ consistent with zero within 2σ, and (3) no thermal excursions exceed ± 1 μK at the absorber.

11. Calibration Strategy

11.1. Photon-Number Calibration

Inject calibrated microwave pulses with known photon number $\bar{n}$:

$$Q_{\text{cal}} = \bar{n} \cdot \hbar\omega_r. \tag{31}$$

For $\omega_r/2\pi = 7$ GHz and $\bar{n} = 1$: $Q_{\text{cal}} = 4.64 \times 10^{-3}$ zJ. This provides an absolute energy scale.

11.2. Heater-Pulse Calibration

Use an on-chip resistive heater to inject known Joule energy $Q_{\text{heater}} = \int I^2(t) R \, dt$. Fit the resulting waveform to extract τ_{th} and validate the linear impulse response $h(t)$. This sets the maximum f_{rep} and determines whether deconvolution is required.

11.3. Linearity Verification

Sweep $\bar{n}$ from 0.1 to 100 photons and verify $Q_{\text{meas}} = a \cdot \bar{n} + b$. The nonlinearity residual must be characterized at the ΔQ_{target} scale ($\sim 9.57 \times 10^{-5}$ zJ), not merely at the 0.1 zJ scale.

11.4. Branch Matching and Common-Mode Rejection

Inject identical calibration pulses upstream of the routing element and verify that the inferred energy is independent of ON/OFF state. Define a balance parameter:

$$\epsilon_{\text{bal}} = \frac{\langle \hat{Q} \rangle_{\text{ON}} - \langle \hat{Q} \rangle_{\text{OFF}}}{\langle \hat{Q} \rangle_{\text{ON}}}. \tag{32}$$

Residual common-mode bias is then $\delta Q_{\text{cm}} \approx \epsilon_{\text{bal}} \, Q_{\text{cm}}$, which must be propagated into the systematic error budget. We require $\epsilon_{\text{bal}} < 10^{-4}$ to keep systematic bias below the signal.

This corresponds to a common-mode rejection ratio (CMRR) of ≥ 80 dB, distinct from the ≥ 40 dB *isolation* between ON/OFF paths (which prevents thermal crosstalk). We reach $\epsilon_{\text{bal}} < 10^{-4}$ in two steps:

Step 1 (VNA pre-calibration). Match amplitude to < 0.01 dB ($\sim 10^{-3}$ fractional), phase to $< 0.5^\circ$, and path-length to < 0.1 mm (< 0.3 ps timing skew). This brings $\epsilon_{\text{bal}} \lesssim 10^{-3}$.

Step 2 (calorimetric closure). Inject identical calibration pulses through both branches and measure ΔQ via the lock-in chain. Trim with precision attenuators and phase shifters, iterate until the calorimetric differential satisfies $|\delta Q_{\text{cm}}| < 0.1 \cdot \Delta Q_{\text{target}}$, corresponding to $\epsilon_{\text{bal}} < 10^{-4}$. This second step compensates residual mismatch that VNA calibration alone cannot resolve.

11.5. Thermal Crosstalk Measurement

With the OFF branch blocked (forcing the pointer to always dissipate), measure any apparent heat in the OFF channel:

$$\eta_{\text{crosstalk}} \equiv \frac{Q_{\text{OFF,blocked}}}{Q_{\text{ON}}}. \tag{33}$$

We require $\eta_{\text{crosstalk}} < 0.01$ ($< 1\%$). For the absolute bias budget, the crosstalk-induced systematic is $\delta Q_{\text{xt}} = \eta_{\text{crosstalk}} \cdot Q_{\text{ON}}$. With $Q_{\text{ON}} \sim \bar{n}\hbar\omega \approx 4.64 \times 10^{-3}$ zJ (single 7 GHz photon) and $\eta < 0.01$, this gives $\delta Q_{\text{xt}} < 4.64 \times 10^{-5}$ zJ, which is below $\Delta Q_{\text{target}} \approx 9.57 \times 10^{-5}$ zJ. For multi-photon pointers ($\bar{n} \gtrsim 10$), a tighter crosstalk bound $\eta < 10^{-3}$ is needed, verified by the same blocked-branch test.

 doi:10.20944/preprints202602.1739.v1

12. Reversibility Witness

Heat alone does not certify objectivity. We implement two complementary metrics.

12.1. Fidelity Metric

Reconstruct the qubit state after an OFF operation and compute

$$\mathcal{F} = |\langle \psi_{\text{initial}} | \psi_{\text{recovered}} \rangle|^2. \tag{34}$$

We distinguish two fidelity criteria. The *hardware design target* is $\mathcal{F} \gtrsim 0.99$ (Sec. 8), which keeps per-shot leakage below the Landauer scale. The *data-quality gate* is a looser $\mathcal{F} > 0.9$, applied to catch catastrophic reversal failures (e.g., quasiparticle events, flux jumps). Shots passing the 0.9 gate but falling below 0.99 contribute a small, characterized systematic (calibrated via Control 3). Shots below 0.9 are discarded. To control for acceptance bias, we (i) verify that the acceptance rate does not depend on the preparation label X or outcome Y, (ii) apply the same fractional random drop to ON shots to confirm $\langle Q \rangle_{\text{ON}}$ is unaffected, and (iii) report $\langle \Delta Q \rangle$ both with and without the fidelity gate to check consistency. Any systematic shift is propagated as a gating-bias uncertainty.

12.2. Operational Metric

As a real-time check, monitor the residual heat in the OFF calorimeter and qubit coherence via echo contrast. A successful uncomputation should yield calorimeter signal consistent with zero (per-shot residual $< \Delta Q_{\text{target}} \approx 9.57 \times 10^{-5}$ zJ after averaging).

12.3. Reversibility Time τ_c

Define τ_c as the smallest delay for which $\mathcal{F}$ drops below 0.9. The calorimetric onset of $\Delta Q > 3\sigma$ at the same timescale is a *separate, independent* observable used to cross-validate the fidelity criterion, not part of the definition. If fidelity loss and heat onset occur at different delays, that discrepancy is itself a diagnostic. τ_c empirically marks the temporal boundary of record formation.

Order-of-magnitude estimate. The reversal protocol requires qubit coherence (for the echo sequence) and pointer coherence (in the storage cavity). The limiting timescale is typically the qubit T_2: for current transmon qubits, $T_2 \gtrsim 50$ μs [11]. The storage cavity lifetime is $\tau_{\text{cav}} = \mathcal{Q}/\omega \approx 1.1$ ms (Sec. 8), which does not limit the protocol. Uncontrolled environmental coupling (substrate phonons, stray radiation, quasiparticle tunneling) degrades the pointer on timescales set by the internal quality factor, typically $\gtrsim 10$ μs for well-isolated superconducting resonators at 10 mK. We therefore estimate $\tau_c \sim 10$ to 50 μs, comfortably above the ~ 100 ns reversal window required by the catch-and-release protocol. The Lindblad simulation (Sec. 5.5) confirms this estimate, yielding $\tau_c \approx 8$ μs with $T_1 = T_2 = 50$ μs and $\mathcal{Q}_{\text{storage}} = 5 \times 10^7$. The ratio $\tau_c / \tau_{\text{reversal}} \approx 78$ provides substantial margin for the OFF-branch uncomputation to complete before environmental decoherence compromises the reversal. Control 3 (Sec. 13) measures τ_c experimentally by sweeping the reversal delay.

13. Controls, Null Tests, and Falsification Criteria

We propose four primary discriminators:

13.1. Control 1: Ground-State Baseline

Prepare the qubit in the ground state $|0\rangle$ across all runs. Here $H(X) = 0$ and $I(X;Y) = 0$.

Prediction: with fixed readout strength, ΔQ is *nonzero* and set by ON-branch pointer absorption, $\Delta Q \approx \bar{n}\hbar\omega_{\text{eff}} - \delta Q_{\text{leak}}$ (up to calibrated branch imbalance). Ground-state preparation sets $I(X;Y) = 0$ but does not remove pointer-energy flow to the ON absorber. This control therefore establishes the nonzero photon-absorption baseline used in residual analysis.

 doi:10.20944/preprints202602.1739.v1

13.2. Control 2: Measurement-Strength Scaling

Prepare a mixed ensemble (e.g., 50% $|0\rangle$, 50% $|1\rangle$) so that $H(X) = 1$. Vary the measurement strength (pointer mean photon number $\bar{n}$) from $\bar{n} \approx 0$ to 1. This sweeps the realized mutual information $I(X;Y)$ from 0 to 1 bit.

Prediction: ΔQ scales linearly with $\bar{n}$, and thus monotonically with $I(X;Y)$. Because $I(X;Y)(\bar{n})$ is generally nonlinear, the relation between ΔQ and $I(X;Y)$ need not be globally linear; the required test is the pointwise inequality $\Delta Q \geq k_B T \ln 2 \cdot I(X;Y)$. In the deep quantum regime, $\Delta Q \sim h\nu$ typically lies far above the Landauer floor, confirming that the energetic cost scales with record-formation strength (Fig. 1).

13.3. Control 3: Reversal-Delay Timing Sweep

Vary the delay τ_d between premeasurement and the uncompute operation in the OFF branch.

Prediction: For $\tau_d < \tau_c$, the OFF branch successfully reverses (high fidelity, low heat), maintaining the full differential signal ($\Delta Q \approx Q_{\text{rec}}$). As τ_d exceeds τ_c, reversal fails, and the OFF branch begins to dissipate, causing ΔQ to degrade toward zero.

13.4. Control 4: Prior-Variation at Fixed Strength

Fix $\bar{n} \approx 1$ (strong measurement) but vary the preparation prior $p(1)$ from 0 to 1.

Prediction: ΔQ tracks the outcome probability $p(1)$ (the population of the absorbing state), while $I(X;Y)$ follows the symmetric entropy curve. The inequality $\Delta Q \geq k_B T \ln 2 \cdot I(X;Y)$ must hold for all priors. This control constrains the state-dependent absorption model used for residual analysis; by itself it does not isolate Landauer-floor saturation in the $h\nu \gg k_B T \ln 2$ regime.

13.5. Auxiliary Null Protocols

Two additional nulls verify hardware systematics:

Toggle-only null. Alternate the routing element between ON and OFF positions while *disabling the dispersive readout pulse* (no pointer created). Any residual ΔQ bounds the heat injected by the switching operation itself.

Pointer-disabled null. Run the full pulse sequence but detune the qubit so that no system-pointer entanglement occurs (pointer in vacuum). Any residual ΔQ bounds routing-path asymmetry at the actual operating frequency.

Both nulls must yield ΔQ consistent with zero within 2σ before production data is collected.

13.6. Falsification Criteria

The record-formation heat bound is **falsified** if, under verified conditions, the pointwise inequality $\langle \Delta Q \rangle_j \geq k_B T \ln 2 \cdot I(X;Y)_j$ fails at any tested operating point j (measurement strength, prior, or temperature), after full uncertainty propagation:

1. For at least one verified point j, the residual $r_j \equiv \langle \Delta Q \rangle_j - k_B T \ln 2 \cdot I(X;Y)_j$ is negative with $> 3\sigma$ significance, where σ includes both statistical uncertainty ($\propto 1/\sqrt{N}$) and systematic contributions from Table 2.
2. A global weighted test over all points gives a negative mean residual at $> 3\sigma$.
3. Record formation is independently verified while ΔQ fails to exceed the calibrated leakage-corrected baseline expected for the chosen pointer-energy setting.

Conversely, the bound is **confirmed** if all tested points satisfy $r_j \geq 0$ within 3σ, across measurement-strength sweeps, prior variation, and temperature scans. In the deep quantum regime ($h\nu \gg k_B T$), large positive residuals are expected and indicate additional irreversible dissipation in the ON branch not present in the OFF branch (e.g., routing asymmetry, additional thermalization channels). As a secondary diagnostic (not the primary falsification statistic), a fit of $\langle \Delta Q \rangle - \langle \Delta Q \rangle_{C1} = m\, I(X;Y) + b'$ can be reported after Control 1 establishes the baseline $\langle \Delta Q \rangle_{C1}$.

 doi:10.20944/preprints202602.1739.v1

13.7. Systematics Summary

Table 2. Requirement-driven systematics for ΔQ.

Mechanism	Bias term	Mitigation	Verified by
Branch imbalance	$\epsilon_{\mathrm{bal}} Q_{\mathrm{cm}}$	S-parameter matching + calorimetric closure	Upstream pulse test
OFF leakage	δQ_{leak}	Coherent catch-release	Fidelity gating
Switch-only offset	Q_{switch}	Toggle-only null	Pointer-disabled null
Nonlinearity	δQ_{nl}	Heater/pulse calibration	Linearity sweep
Drift	$\delta Q_{\mathrm{drift}}$	Lock-in + PID	Baseline tracking

14. Discussion

14.1. Relation to Prior Work

Bérut *et al.* [15] verified Landauer's principle for classical bit erasure. Our proposal extends this to *quantum* measurement, where the "erasure" is of quantum coherence: the elimination of alternatives during record formation. The key distinction: in classical systems, a pre-existing bit is erased; in quantum measurement, classical information is *created* by eliminating quantum alternatives. For pure-state binary outcomes these scales coincide numerically at $k_{\mathrm{B}} T \ln 2$ per bit; for mixed or partially decohered states they need not. The physical process and bookkeeping differ from classical reset.

14.2. Applicability Summary

Table 3. Landauer bound applicability (assumes C1 to C6).

Stage	Rev.?	$I(X;Y)$?	Landauer?
1 (Premeas.)	Yes	No	**No**
2 (Record)	No	Yes	**Yes**
3 (Reset)	No	Erased	Yes

14.3. Theoretical Necessity

The thermodynamic cost measured here is not accidental. A companion theoretical work [19] demonstrates that the Born rule ($P = |\psi|^2$) is the unique probability assignment consistent with the erasure of quantum phase information required to form a classical record. This experiment thus probes the energetic price of the transition from quantum amplitude to classical probability.

14.4. Implications

A positive result would establish measurement as a thermodynamic event with a quantifiable heat signature, providing an operational criterion: *objective record formation under C1 to C6 occurs when the dissipative cost is paid*. This complements interpretational frameworks (Copenhagen, Many-Worlds, decoherence) with a physical observable.

15. Conclusion

We have provided a unified operational theory-experiment package:

1. A three-stage taxonomy separating reversible premeasurement, irreversible record formation, and memory reset, with six explicit operational conditions (C1 to C6) specifying when the Landauer bound applies.
2. A conditional record-formation heat bound $\langle Q_{\mathrm{rec}} \rangle \geq k_{\mathrm{B}} T \ln 2 \cdot I(X;Y)$, derived from the generalized second law and anchored by an explicit system/pointer/bath model. The model locates dissipation at record formation (Stage 2, environmental coupling), not at premeasurement (Stage 1, unitary correlation), with a protocol-dependent heat/work split made explicit by C1 to C6.

 doi:10.20944/preprints202602.1739.v1

3. A differential microcalorimetry experiment using matched ON/OFF branches, lock-in modulation, and reversibility witnesses, with a complete calibration/systematics program.

The protocol uses demonstrated thermal-detector qubit readout and is compatible with existing circuit-QED infrastructure. Four primary controls discriminate the predicted signal from backgrounds. Sensitivity analysis using nanobolometer performance shows SNR $\gtrsim 10$ is achievable at 10 mK; integration time depends on detector bandwidth and modulation rate. Landauer-scale residual tests at 10 mK remain experimentally demanding (hours to weeks, depending on detector thermal time and effective modulation rate), while deep-quantum operation with $\Delta Q \sim h\nu \gg k_B T \ln 2$ is already comfortably accessible. All computable numerical values in this manuscript are generated or cross-validated by the accompanying scripts `Simulations/simulation.py`, `Simulations/qutip_simulation.py`, and `Simulations/run_full_audit.py`.

A positive result would establish an experimentally anchored thermodynamic criterion for objective quantum measurement.

Data Availability Statement: The numerical data and figures analyzed in this study are generated by the accompanying simulation and audit scripts in the `Simulations/` directory. Derived outputs (including audit summaries and QuTiP reports) are reproducible by running `simulation.py`, `qutip_simulation.py`, and `run_full_audit.py` with the repository defaults.

Acknowledgments: The author thanks colleagues for helpful discussions.

References

1. R. Landauer, "Irreversibility and Heat Generation in the Computing Process," IBM J. Res. Dev. **5**, 183 (1961).
2. C. H. Bennett, "Notes on Landauer's principle, reversible computation, and Maxwell's Demon," Stud. Hist. Phil. Mod. Phys. **34**, 501 (2003).
3. J. D. Norton, "Waiting for Landauer," Stud. Hist. Phil. Mod. Phys. **42**, 184 (2011).
4. J. Ladyman and K. Robertson, "Landauer defended: Reply to Norton," Stud. Hist. Phil. Mod. Phys. **48**, 210 (2014).
5. T. Sagawa and M. Ueda, "Minimal Energy Cost for Thermodynamic Information Processing: Measurement and Information Erasure," Phys. Rev. Lett. **102**, 250602 (2009).
6. M. Cortês and A. R. Liddle, "Hawking evaporation and the Landauer Principle," arXiv:2407.08777 (2024).
7. W. H. Zurek, "Quantum Darwinism," Nature Phys. **5**, 181 (2009).
8. A. Touil, B. Yan, D. Girolami, S. Deffner, and W. H. Zurek, "Quantum Darwinism, Amplification, and the Origin of Objective Classical Reality," Phys. Rev. Lett. **128**, 010401 (2022).
9. C. L. Latune and C. Elouard, "A thermodynamically consistent approach to the energy costs of quantum measurements," Quantum **9**, 1614 (2025).
10. M. H. Mohammady and F. Buscemi, "The thermodynamic trilemma of efficient measurements," Quantum **9**, 1250 (2025).
11. N. Katz *et al.*, "Reversal of the weak measurement of a quantum state in a superconducting phase qubit," Phys. Rev. Lett. **101**, 200401 (2008).
12. A. M. Gunyhó *et al.*, "Single-shot readout of a superconducting qubit using a thermal detector," Nat. Electron. **7**, 288 (2024).
13. R. Kokkoniemi *et al.*, "Nanobolometer with ultralow noise equivalent power," Commun. Phys. **2**, 124 (2019).
14. J. P. Pekola *et al.*, "Ultrasensitive Calorimetric Detection of Single Photons from Qubit Decay," Phys. Rev. X **12**, 011026 (2022).
15. A. Bérut *et al.*, "Experimental verification of Landauer's principle linking information and thermodynamics," Nature **483**, 187 (2012).
16. Y. Yin *et al.*, "Catch and Release of Microwave Photon States," Phys. Rev. Lett. **110**, 107001 (2013).
17. F. Wulschner *et al.*, "Tunable coupling of transmission-line microwave resonators mediated by an rf SQUID," EPJ Quantum Technol. **3**, 10 (2016).
18. J. R. Johansson, P. D. Nation, and F. Nori, "QuTiP 2: A Python framework for the dynamics of open quantum systems," Comp. Phys. Commun. **184**, 1234 (2013).
19. M. Rahnama, "Born's Rule from Record-Formation Constraints: A Thermodynamic-Information Axiomatics," (2026), submitted.

 doi:10.20944/preprints202602.1739.v1

20. M. Rahnama, "Landauer Saturation in Hawking Evaporation and an Information and Energy Accounting Framework," (2026), submitted.